AIAA JOURNAL
Vol. 34, No. 2, February 1996

Direct Numerical Simulation of Acoustic/Shear Flow Interactions in Two-Dimensional Ducts

Siming Mu* and Shankar Mahalingam†
University of Colorado, Boulder, Colorado 80309-0427

The interaction between an imposed monochromatic, time-dependent acoustic disturbance and a steady mean shear flow in a two-dimensional duct is studied using direct numerical simulation. Unlike previously reported numerical results, the long-time acoustic response is captured through implementation of accurate nonreflecting boundary conditions. Below a certain cutoff frequency, the acoustic field is a nearly planar traveling wave propagating axially along the duct. Above this cutoff frequency, oblique waves are generated due to both acoustic refraction and cross-stream dependent source oscillation, leading to an alternating pattern of higher acoustic pressures at the wall and the centerline, downstream of the disturbance source. At resonant conditions, the growth of the oblique wave, which is nearly transverse, dominates the axial wave, leading to a phase change of 180 deg after their interaction. The thickness of the acoustic boundary layer and its response to imposed disturbances are also in good agreement with theory. These results are consistent with previously published theoretical predictions and represent their first numerical verification.

Nomenclature

a_∞	= reference speed of sound, also reference velocity
C_p	= constant pressure specific heat, temperature independent
e_t	= internal energy per unit volume
h	= duct half-width
i, j, k	= coordinate directions in Cartesian tensor notation
L	= computational length of duct
M	= mean flow Mach number
Pr	= Prandtl number
p	= pressure
q_j	= heat flux vector component in the jth direction
Re	= acoustic Reynolds number in the calculation
Re_c	= duct Reynolds number
T	= temperature
t	= time variable
u_k	= velocity component in the kth coordinate direction
$\hat{u}$	= axial acoustic velocity disturbance
v	= velocity component in the y coordinate direction
x, y	= spatial variables along the x and y coordinate directions
x_j	= independent spatial variable along the jth coordinate direction
α	= computational duct aspect ratio
γ	= constant specific heat ratio
δ	= acoustic boundary-layer thickness
ϵ	= small parameter used in perturbation analysis
κ	= viscosity power law exponent
μ	= coefficient of dynamic viscosity
ν	= coefficient of kinematic viscosity
τ_{ij}	= stress tensor
Ω	= dimensionless frequency of imposed oscillation

Subscripts

∞	= reference quantity, chosen at stagnant conditions
s	= undisturbed steady state

Superscripts

$\hat{}$	= acoustic disturbance
$'$	= dimensional quantity

Received Nov. 26, 1994; revision received April 17, 1995; accepted for publication April 20, 1995.

*Graduate Student, Department of Mechanical Engineering, Center for Combustion Research.
†Assistant Professor, Department of Mechanical Engineering, Center for Combustion Research. Member AIAA.

Introduction

THE interaction of an acoustic wave disturbance with a shear flow provides a mechanism for transfer of energy between the mean and various modes of the acoustic flow. This problem is significant as it provides a vital link in the chain of events that could lead to combustion-driven acoustic instability in solid rocket motors. However, in practical motors, the various mechanisms that contribute to amplification and damping of acoustic energy are intimately related to the acoustic mode and the type of propellant lining the motor surface.[1] This makes it difficult to isolate physical mechanisms associated with individual processes when the full problem is investigated. Thus, the focus of this paper is on the mechanism of energy exchange between the mean and various modes of the acoustic flow in a sufficiently simplified flow situation for which theoretical results are available. This problem is investigated via direct numerical simulation (DNS) of the interaction between an imposed acoustic velocity disturbance in an otherwise steady shear flow established in a two-dimensional duct. In DNS, the complete time-dependent system of equations is solved without any explicit modeling, such as turbulence modeling. This procedure has been successfully applied to a variety of incompressible, compressible, and reacting flows.[2]

Much of past analytical work has focused on obtaining quasisteady solutions to a linearized wave equation describing acoustic wave propagation in a fully developed duct flow.[3] Using this as a basis, both downstream propagating[3] and upstream propagating acoustic waves[4,5] have been investigated. Results suggest that, in the former case, the acoustic pressure at the wall is larger than that at the centerline; the reverse is true in the latter case. Since this method presumes the form of the solution, it cannot predict the evolution from an initial disturbance to the quasisteady form. Baum and Levine[6] and, subsequently, Wang and Kassoy[7] proceeded to rectify this shortcoming by investigating an initial boundary value problem, albeit using entirely different approaches. Baum and Levine solved the compressible Navier–Stokes equations numerically for a Reynolds number, based on centerline velocity and duct width, of approximately 10^5. A turbulence model was included in their calculations. A disturbance was introduced at a certain cross section, and its evolution was tracked. They found that acoustic refraction effects increased with the frequency of the imposed disturbance. The relationship between the wall and centerline acoustic pressure for upstream and downstream propagation of acoustic waves, in a qualitative sense, was consistent with that predicted by the quasisteady theory.[4,5] At the outflow boundary, they had difficulty in prescribing nonreflecting conditions, and hence they terminated their computations when the imposed wave reached the downstream boundary of

their computational domain. Thus the long-time transient solution, which has since been demonstrated to be extremely important,[7] was not available in their work. This may also be the reason why they did not observe oblique waves and resonant mode oscillations. Using a rational perturbation procedure, Wang and Kassoy[7] solved an initial boundary value problem to describe acoustic processes in a two-dimensional shear flow in a duct for small mean flow Mach number and large Reynolds number. Their results indicate that, as a result of leading order axial wave refraction by the shear flow, oblique propagating waves develop. This refraction effect increases with the driving frequency of the imposed acoustic disturbance and the mean flow Mach number. The oblique waves evolve into purely amplifying transverse waves at frequencies corresponding to resonance. The initial boundary value approach just discussed differs from what may be termed a normal mode analysis that is often applied to problems involving combustion-driven acoustic instability in solid rocket motors[8–10] and pulsed combustors.[11] In the traditional approach,[8–10] the amplitudes of either the classical acoustic modes or modes suitably modified to account for processes that influence the basic acoustic modes are described via an infinite system of coupled ordinary differential equations. The idea is then to obtain conditions that could lead to growth or amplification of different modes and also to predict conditions that could lead to limit-cycle-type behavior.

The objective in the present paper is to verify the existence of and to understand the role of oblique waves generated through acoustic refraction when a monochromatic, acoustic velocity disturbance introduced at a fixed duct location is allowed to interact with a steady shear flow in a two-dimensional duct. In particular, we seek to validate the analytical results obtained by Wang and Kassoy[7] and to use their predictions to examine and interpret the complex acoustic structure that is obtained. The approach adopted is an accurate solution to the compressible Navier–Stokes equations through DNS of the problem.

Problem Formulation

The full compressible two-dimensional Navier–Stokes equations are solved as an initial value problem using a code originally developed by Baum and Poinsot[12] for reacting flows and adapted for the present research. The computational domain and coordinate system are represented in Fig. 1. The equations are rendered dimensionless using the duct length L, speed of sound at stagnant conditions a_∞, the corresponding density ρ_∞, and the dynamic pressure $\rho_\infty a_\infty^2$. The reference temperature is $(\gamma - 1)T_\infty$. The reference viscosity used is $\mu_\infty = \mu(T_\infty)$. The reference time is thus the acoustic time L/a_∞. The dimensionless parameters governing the problem are the Reynolds number defined as

$$Re = \frac{\rho_\infty a_\infty L}{\mu_\infty} \tag{1}$$

and the Prandtl number $Pr = \mu_\infty C_p/\lambda_\infty$, where $\lambda_\infty = \lambda(T_\infty)$. Note that the duct aspect ratio defined as

$$\alpha = L/2h \tag{2}$$

although not a parameter, appears in the analysis since the computational domain is finite. By applying nonreflecting boundary conditions as discussed in the next section, the flowfield in a duct of infinite length is effectively simulated. Henceforth all quantities are dimensionless. Dimensional quantities where appropriate are indicated by a prime. The dimensionless form of the governing equations written in Cartesian tensor notation appears next.

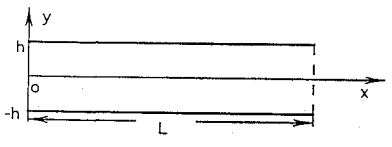

Fig. 1 Schematic representation of model problem. The mean flow is along the x' axis. Acoustic perturbations are imposed at $x' = 0$. Nonreflecting boundary conditions are imposed at $x' = L$.

Continuity:

$$\frac{\partial \rho}{\partial t} + \frac{\partial \rho u_j}{\partial x_j} = 0 \tag{3}$$

Momentum:

$$\frac{\partial \rho u_i}{\partial t} + \frac{\partial \rho u_i u_j}{\partial x_j} = -\frac{\partial p}{\partial x_i} + \frac{1}{Re}\frac{\partial \tau_{ij}}{\partial x_j} \tag{4}$$

Energy:

$$\frac{\partial \rho e_t}{\partial t} + \frac{\partial (\rho e_t + p)u_j}{\partial x_j} = \frac{1}{Re}\frac{\partial (u_i \tau_{ij})}{\partial x_j} - \frac{1}{RePr}\frac{\partial q_j}{\partial x_j} \tag{5}$$

The internal energy per unit volume is given by

$$e_t = \frac{1}{2}\rho u_k u_k + \frac{p}{\gamma - 1} \tag{6}$$

The stress tensor τ_{ij} and the heat flux vector q_j are taken for a Newtonian fluid with the Fourier model for heat conduction as follows:

$$\tau_{ij} = \mu\left(\frac{\partial u_i}{\partial x_j} + \frac{\partial u_j}{\partial x_i} - \frac{2}{3}\delta_{ij}\frac{\partial u_k}{\partial x_k}\right), \qquad q_i = -\lambda\frac{\partial T}{\partial x_i} \tag{7}$$

The dynamic viscosity μ is dependent on temperature such that $\mu \sim T^\kappa$, where the exponent κ is a constant. The thermal conductivity λ is related to the dynamic viscosity through the constant Prandtl number. The equation of state is

$$p = \rho T \frac{\gamma - 1}{\gamma} \tag{8}$$

Numerical Method and Boundary Treatment

A compact sixth-order accurate finite difference scheme developed by Lele[13] is used to approximate the first and second derivatives in the governing equations. The order of accuracy is fourth and third, respectively, at points adjacent to and on the boundary of the computational domain. This scheme requires solution of a tridiagonal matrix to compute the derivatives. The advantage of the compact scheme over more familiar finite difference schemes is that it provides spectral-like resolution of both the amplitude and phase of the solution, thereby enabling the scheme to accurately capture acoustic wave behavior. A complete analysis of this scheme including a comparison of dispersion errors with traditional finite difference schemes is presented by Lele.[13] A third-order explicit Runge–Kutta scheme is adopted for time advancement of the semidiscrete equations.

One critical requirement for capturing the wave characteristics of the acoustic field is accurate treatment of boundary conditions. In the present paper, a systematic boundary treatment method, namely, Navier–Stokes characteristic boundary condition (NSCBC), is utilized.[14] Based on the idea of characteristics for Euler equations,[15] the NSCBC assumes that the waves propagated by Navier–Stokes equations are associated with only the hyperbolic part of the equation.[14] Thus the first derivative normal to a boundary appearing in the convective term of the Navier–Stokes equations may be rewritten in terms of the amplitude variations of the characteristic waves represented by Navier–Stokes equations. For those characteristic waves propagating out of the domain, the values of their amplitude variation are completely defined by data from within the computational domain through use of one-sided approximations. Numerical stability is achieved since this amounts to upwind differencing. For those waves propagating into the computational domain, boundary conditions are needed to specify the values of their amplitude variations. There is no exact method to compute the amplitude variations of these incoming waves. A set of locally one-dimensional inviscid (LODI) equations are used to infer the values of the incoming amplitude variations from the boundary conditions. Derivatives parallel to the boundary pose no problems and are treated exactly as in the interior. The treatment of viscous conditions is based on the method suggested in Ref. 14. These terms go to zero as the viscosity

goes to zero. For a detailed discussion of the NSCBC procedure, the paper by Poinsot and Lele[14] may be consulted.

In this paper the flow considered is subsonic with a mean flow Mach number $M \approx 0.08$. Unless otherwise noted, $\alpha = 5$, $Re = 2 \times 10^4$, and $Pr = 1$. Thus the Reynolds number based on the mean flow velocity and duct width $Re_c = MRe/\alpha = 320$.

Reflecting boundary conditions are used at the inlet. The transverse velocity component v is set to zero; the axial velocity profile $u = u(0, y, t)$, such that $u(0, -\frac{1}{2\alpha}, t) = u(0, +\frac{1}{2\alpha}, t) = 0$, is prescribed; and a constant inlet temperature, $T(0, y, t) = 1/(\gamma - 1)$ is prescribed. At the lateral boundary, no-slip velocity and isothermal conditions are prescribed. At the outflow, nonreflecting boundary conditions based on the method developed in Ref. 14 are imposed. This allows acoustic waves to propagate out of the domain with little or no reflections and thus enables us to carry out long-time stable computations. A steady flow is established by initializing the domain with stagnant flow and raising the pressure at the inlet by 5% of the initial uniform pressure, $p = 1$. This steady-state flowfield is used as initial conditions for several transient problems in which a time-dependent perturbation is imposed on the incoming streamwise velocity.

Results and Discussion

Code Validation

Several test problems were simulated to verify that the code and boundary condition treatment are satisfactory. Both nonreflecting and reflecting boundary conditions were examined.[16] To test the NSCBC procedure, a very viscous test problem[14] was simulated. The inlet conditions imposed are

$$u(0, y, t) = u_0 \cos^2(\pi y \alpha), \qquad v(0, y, t) = 0, \qquad T(0, y, t) = T_0 \tag{9}$$

where u_0 and T_0 are constants. Nonreflecting conditions are imposed at the outlet. The Reynolds number $Re = 2 \times 10^3$ and a uniform 41×41 mesh was used. Steady-state contour plots of u/u_0, $100(p - p_\infty)/p_\infty$, and $100(T - T_\infty)/T_\infty$ are virtually identical to past numerical[14] and analytical results,[14] thereby validating the code and boundary conditions. For the sake of brevity, in Fig. 2, only contour plots of temperature are presented. Transient results presented in the remainder of this section were obtained on a uniform 81×81 mesh. Grid independence was verified by repeating the calculations on a 161×161 grid. All calculations were performed on a Cray C-90 at the San Diego Supercomputing Center.

Nature of Imposed Disturbance

A transient acoustic field is generated by imposing a single frequency disturbance on the inlet axial velocity. No slip at the lateral walls demands that the amplitude of the disturbance be zero at $y = \pm\frac{1}{2\alpha}$. Although the analysis in Ref. 7 is quite general, the results the authors present are for constant amplitude and linear variation of amplitude, and thus our results can only be qualitatively related to their theoretical results. The axial velocity disturbance $\hat{u}(y, t)$ was chosen to have the following mathematical form:

$$\hat{u}(y, t) = AU(y)\sin\left[\alpha\pi\left(y + \frac{1}{2\alpha}\right)\right]\sin \Omega t \tag{10}$$

where Ω is defined through $\Omega = \Omega' L/a_\infty$, and $U(y)$ is the initial, steady axial velocity at the inlet. The quantity A is a constant that controls the magnitude of the disturbance. The disturbance is introduced by specifying an axial inlet velocity profile of the form

$$u(0, y, t) = U(y) + \epsilon\hat{u}(y, t) \tag{11}$$

The quantity ϵ is the small parameter introduced in Ref. 7. By performing a fast Fourier transform (FFT) in y on the discrete version of Eq. (10), it is found that the primary transverse mode components are the zeroth and first modes, with higher mode amplitudes being less than 2% of these. Thus it is reasonable to expect that the simulation results will compare well with Ref. 7, at least qualitatively.

Theory[7] for y-independent amplitude function suggests that for $\Omega < \alpha n\pi$, $n = 1, 2, 3, \ldots$, only axial waves would exist. When $\Omega > \alpha n\pi$, refraction-induced oblique waves begin to appear. In the present simulation $\alpha = 5$, and since the mean flow is symmetric with respect to the duct center plane, only even values of n are relevant. This leads to the first cutoff frequency of 10π (corresponding to $n = 2$) above which oblique waves are expected to be generated. The leading order solution is uninfluenced by the mean flow except through a bulk convection effect. Through an examination of the second-order acoustic solution Wang and Kassoy[7] predicted that $\Omega = \alpha n\pi$ corresponds to resonant conditions. Classical quasi-steady theory[3] cannot describe resonant oscillations, and previous numerical simulations were unable to capture this phenomenon due to difficulties in implementing outflow boundary conditions.[6] The numerical solutions were curtailed when the disturbance reached the outflow boundary, and hence the long-time behavior, required to observe resonant effects, was not studied.[6,7] In the present work, several frequencies were examined. In the following subsections, results are presented for different values of Ω that were chosen to represent typical characteristics of different frequency regimes. Since the no-slip wall condition in the simulations demands that the perturbation amplitude be y dependent, it is important to recognize that higher modes (nonplanar) are expected to be generated directly by the source, in addition to refraction of the planar component.[7] Using the decomposition in Ref. 7, the total acoustic pressure $\hat{p}$ and axial acoustic velocity $\hat{u}$ were obtained as

$$\hat{p} = (1/\gamma M\epsilon)\,[p(x, y, t) - p_s(x, y)]$$
$$\hat{u} = (1/\epsilon)\,[u(x, y, t) - u_s(x, y)] \tag{12}$$

where p_s and u_s are the undisturbed steady pressure and axial velocity, respectively. In all cases, computations were carried out up to four acoustic time units, with $\epsilon = 0.1$.

Acoustic Pressure Field for $\Omega = 10$

The frequency $\Omega = 10$ is below the first cutoff frequency of 10π. Figure 3 represents the total acoustic pressure time history at $x = 0.6$. For convenience, the time scale used by Wang and Kassoy[7]

$$t_w = t'\Omega' \tag{13}$$

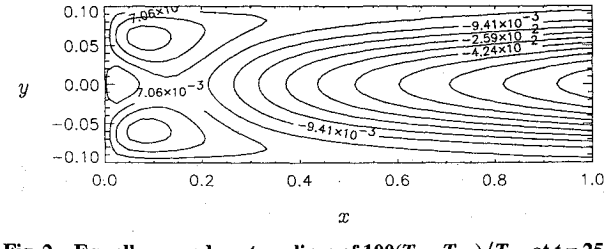

Fig. 2 Equally spaced contour lines of $100(T - T_\infty)/T_\infty$ at $t = 25$ and $Re = 2 \times 10^3$.

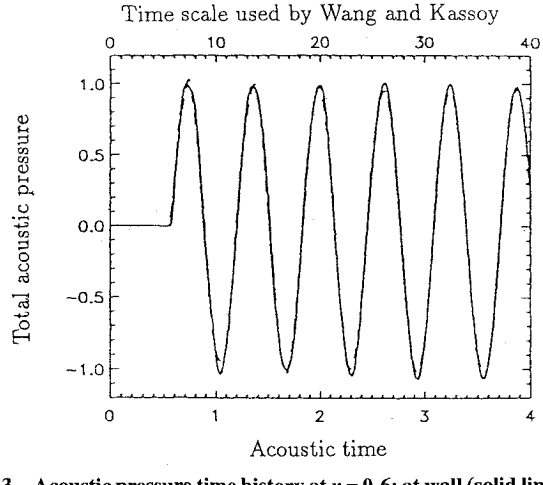

Fig. 3 Acoustic pressure time history at $x = 0.6$: at wall (solid line) and center (dashed line); $\Omega = 10$, mesh = 81×81, and $Re = 2 \times 10^4$.

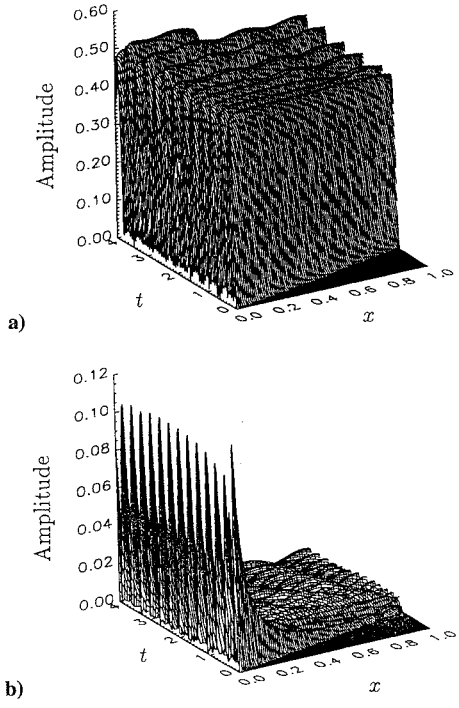

Fig. 4 Amplitudes of a) zeroth and b) first transversal spatial mode component of acoustic pressure for $\Omega = 10$, mesh = 81 × 81, and $Re = 2 \times 10^4$.

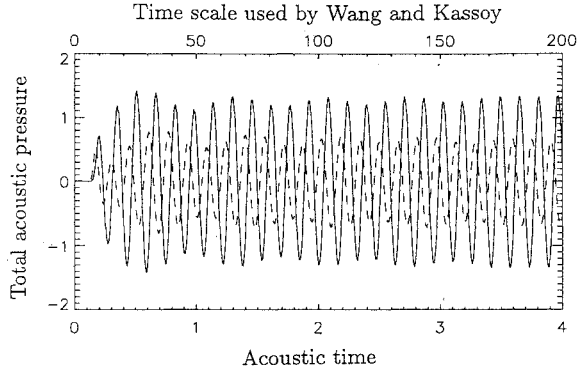

Fig. 5 Acoustic pressure time history at $x = 0.15$—center (dashed) and wall (solid)—for $\Omega = 40$ and $Re = 2 \times 10^4$.

where t' is the dimensional time is also shown in Fig. 3. The amplitude of acoustic pressure at the centerline is slightly smaller than that at the wall (also true at other x locations) due to refraction of the downstream propagating acoustic wave. An examination of acoustic pressure contours suggests that sufficiently far downstream from the inlet the waves are nearly planar. Thus no oblique waves appear for the conditions of the simulation. This result is in qualitative agreement with analytical prediction.[7] An FFT analysis of the acoustic pressure with respect to y at various axial locations and times (see Fig. 4) shows a dramatic decay in amplitudes of the first transversal spatial component, whereas very little decay in amplitudes is seen for the zeroth component. Since the latter corresponds to the planar part of the disturbance, this result is consistent with the earlier remark that, at locations sufficiently far downstream from the disturbance source, only the planar component survives.

Acoustic Pressure Field for $\Omega = 40$

The forcing frequency $\Omega = 40$ is just above the first cutoff frequency. The acoustic pressure time history at fixed locations is presented in Fig. 5. A comparison of Fig. 5 with Fig. 3 reveals several interesting features. At early times, after the first arrival of the waves, an increase in amplitude can be observed. Then the amplitudes themselves begin to oscillate, although at a much reduced frequency. Recall from Ref. 7 that a plane wave

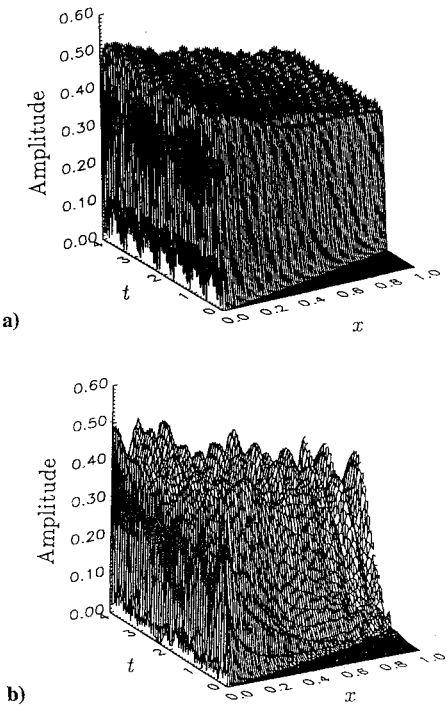

Fig. 6 Amplitudes of a) zeroth and b) first transversal spatial mode component of acoustic pressure for $\Omega = 40$ and $Re = 2 \times 10^4$.

(zeroth transversal spatial mode) with its frequency above the cutoff frequency generates oblique waves as it travels downstream. In the present work, the acoustic source is nonplanar due to the y-dependent amplitude function, and thus oblique waves are expected to be excited, in addition to refraction of the axial mode giving rise to oblique waves. The result of these two processes is a variation in amplitudes of acoustic pressure as depicted in Fig. 5. Further it is evident from Fig. 5 that the pressure amplitude for $\Omega = 40$ is greatly enhanced compared with that for $\Omega = 10$ (see Fig. 3). This enhancement arises from the increased amplitudes of the first transversal spatial mode as can be seen from Figs. 6a and 6b. From these plots it is apparent that the amplitudes of the first transversal spatial mode grow to values having the same order as those of the zeroth mode, whereas the amplitudes of the zeroth mode vary very little compared with those for $\Omega = 10$.

Acoustic Pressure Field for $\Omega = 10\pi$

The angular frequency $\Omega = 10\pi$ corresponds to the second resonant mode. Figure 7 depicts the acoustic pressure time history at the wall and centerline at different axial locations. The general feature of resonant oscillation is displayed at locations (1c) and (1w) (here w and c denote wall and centerline, respectively), where the acoustic pressure amplitudes increase consistently with time. However, axial stations 2 and 3 display slightly different features. One can see that at some axial locations (stations 2w, 3w, and 4c) the signal initially decreases and subsequently increases. This behavior is very similar to that reported by Wang and Kassoy.[7] Although Wang and Kassoy[7] focus their discussion on second-order acoustic pressure, their qualitative description is also valid for the total acoustic pressure because the first-order acoustic pressure is just a plane sine wave propagating axially, for y-independent source amplitude. The acoustic pressure amplitude at different axial stations increases with time after sufficient time elapses. However, the amplitude of acoustic pressure may initially decrease with time "owing to destructive interference."[7] Previous numerical investigation by Baum and Levine[6] was limited to very short time solution due to difficulties alluded to earlier. Both the present numerical and previous analytical results show that an examination of the short-time solution is insufficient to conclude whether resonant amplifications are occurring.

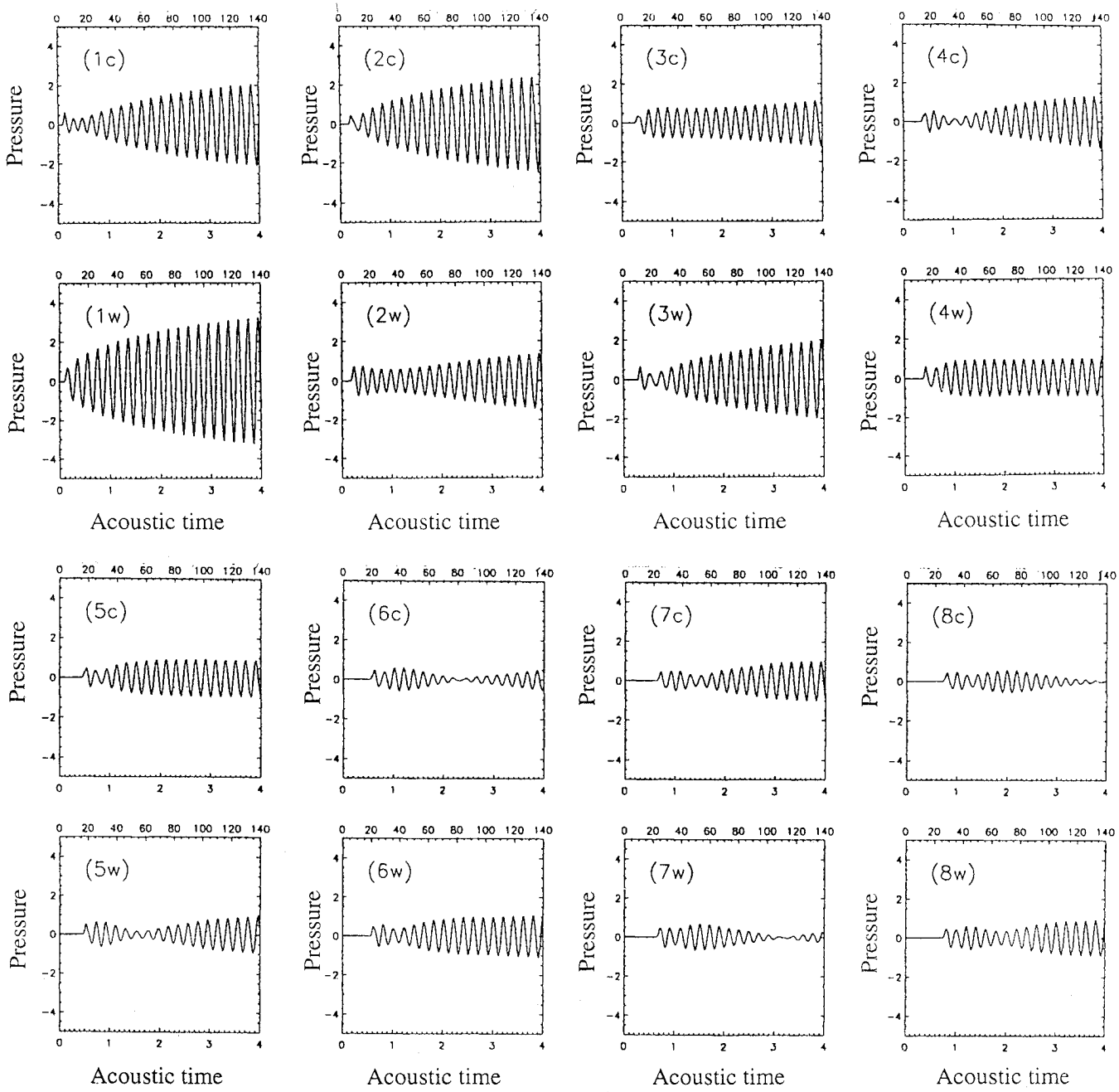

Fig. 7 Acoustic pressure time history at different locations; c: centerline and w: wall. (1) $x = 0.1$, (2) $x = 0.2$, (3) $x = 0.3$, (4) $x = 0.4$, (5) $x = 0.5$, (6) $x = 0.6$, (7) $x = 0.7$, and (8) $x = 0.8$ for $\Omega = 10\pi$ and $Re = 2 \times 10^4$. Note that the acoustic time scale is 0 to 4 (0 to 140 in the time scale used by Wang and Kassoy[7]), and the scale for acoustic pressure is −5 to 5 in all of the figures.

Acoustic pressure data at downstream locations (stations 4–8 in Fig. 7) reveal some additional features that have not been reported previously. After the initial decrease in amplitude due to destructive interference, the amplitudes at all locations start to increase with time. Then at some locations wave amplitudes quickly stop amplifying and remain nearly constant, suggesting that extraction of acoustic energy (to the mean) and viscous dissipation are occurring. On the other hand, at other locations amplitudes start to decrease again and eventually reach a value close to zero. When the acoustic pressure amplitudes increase once again, they have undergone a phase change of π with respect to the phase of the signal at early time. This can be seen by overlaying the data from locations (6c) and (6w) of Fig. 7, not included here for the sake of brevity. This behavior of acoustic pressure waves suggests an interaction between an axially traveling wave and another much stronger wave that arrives after the axial wave and has an opposite phase with respect to the axial wave. Based on theoretical results,[7] it may be concluded that the alternating appearance of this behavior under resonant conditions is caused by the interaction of axial with nearly transverse waves. Unlike the $\Omega = 40$ case, transverse waves for $\Omega = 10\pi$ are excited and grow with time due to resonance. A pictorial representation of the instantaneous acoustic pressure fields is presented in Figs. 8a–8d. The direction along which the pressure gradient is a maximum is indicative of the instantaneous wave structure as a result of axial and transverse mode interaction. Based on a comparison of the present results with theory,[7] the following observations may be made:

1) Present simulation shows that under resonant conditions significant interaction between the nearly transverse and axial waves only appears downstream, sufficiently far away from the disturbance source probably because the waves need a certain amount of travel distance and time to collect sufficient acoustic energy and settle into nearly transverse waves.

2) From the analysis presented in Ref. 7, where the source amplitude function is y dependent, it is evident that the magnitude of the higher modes is of the same order as the axial mode and the effect

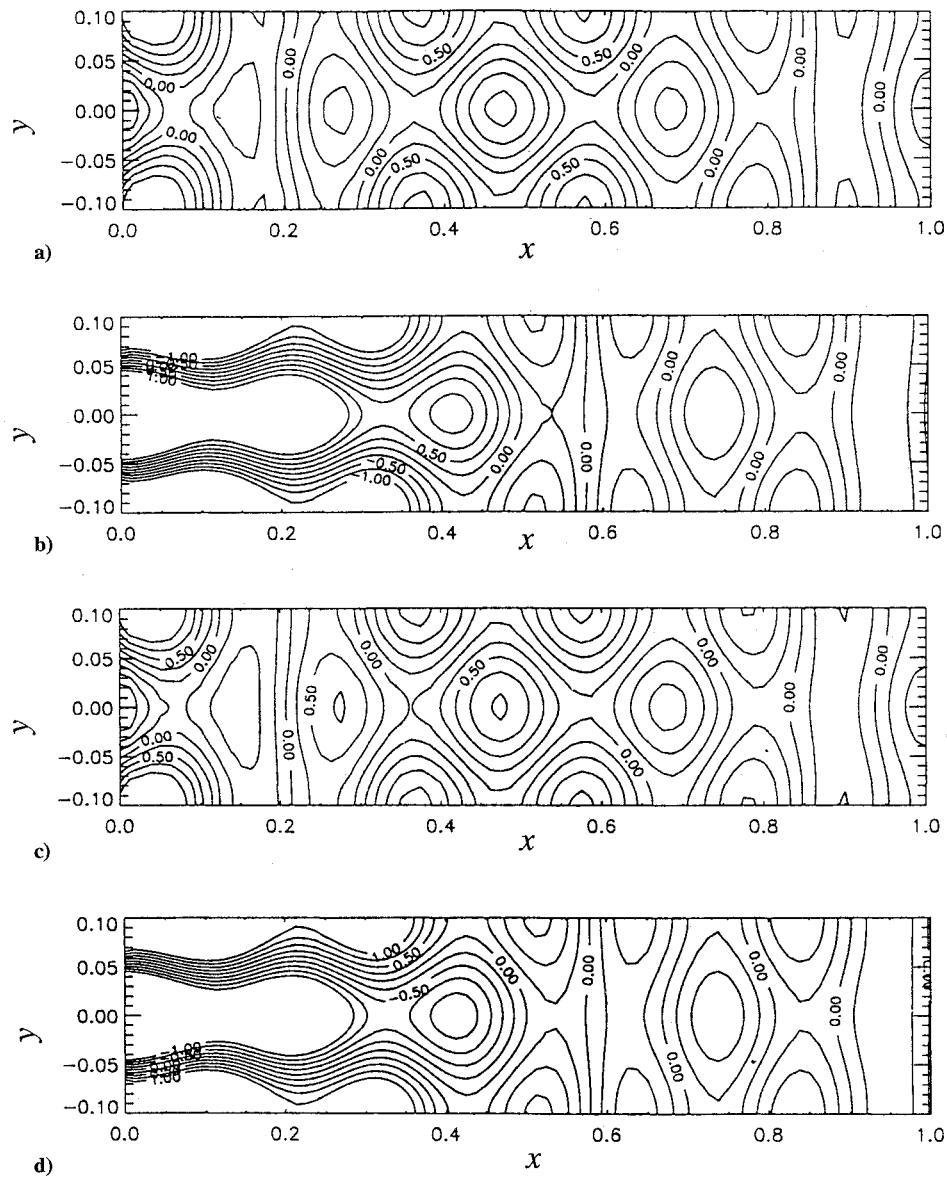

Fig. 8 Acoustic pressure contours (equispaced) at a) $t = 3.0$, b) $t = 3.05$, c) $t = 3.10$, and d) $t = 3.14$ for $\Omega = 10\pi$ and $Re = 2 \times 10^4$.

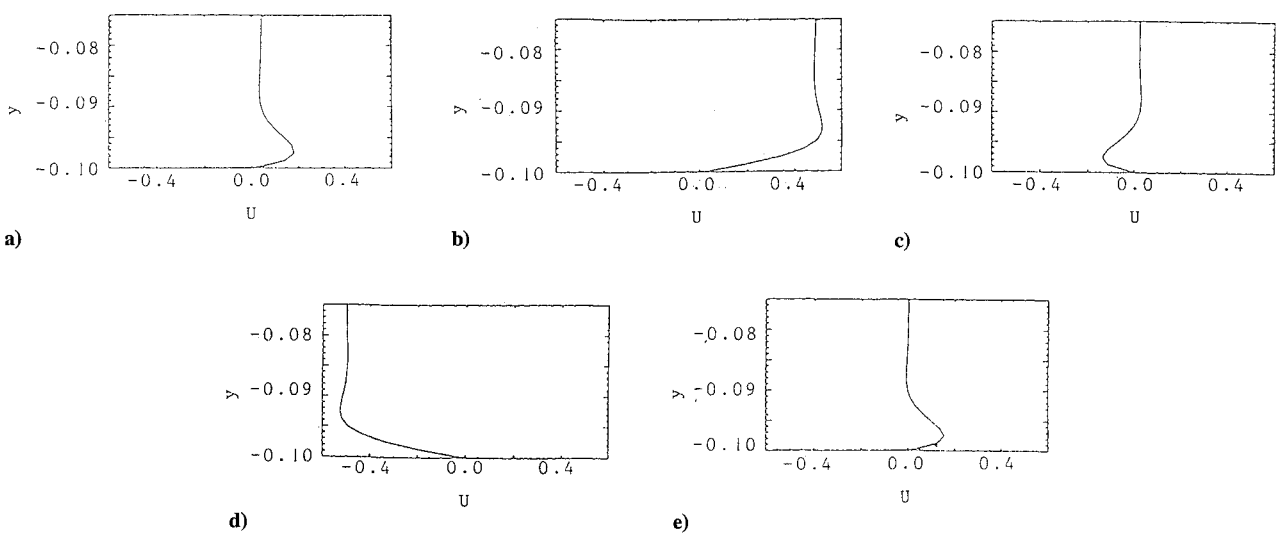

Fig. 9 Axial acoustic velocity profiles at $x = 0.5$ and a) $t = 3.00$, b) $t = 3.14$, c) $t = 3.30$, d) $t = 3.45$, and e) $t = 3.62$ for $\Omega = 10$, mesh = 81×161, and $Re = 2 \times 10^4$. Note that u axis scale is -0.6 to 0.6, and y axis scale is -0.1 to -0.080.

of refraction of the axial mode is of lower order. This suggests that the present results are dominated by the source structure.

Acoustic Boundary Layer

The existence of an acoustic boundary layer is another interesting feature that arises naturally due to the acoustic mean flow interaction. It is a region close to the wall within which an overshoot of axial acoustic velocity can be observed as depicted in Fig. 9. The magnitude of the overshoot reaches a maximum value whenever the axial acoustic velocity in the core changes sign. This phenomenon is attributable to Richardson's annular effect.[6,7] The thickness of the acoustic boundary layer δ is given in Ref. 7 by

$$\delta = 5\left[\frac{M}{\gamma Re_c}\right]^{\frac{1}{2}} \tag{14}$$

This thickness, expressed as a fraction of the duct width, is defined as the distance from the wall where the axial velocity reaches 97.3% of the core value. Approximately eight grid points are present within this boundary layer, a value that is sufficient to resolve the acoustic boundary layer. In the present case, $\delta = 5.6\%$ is the predicted value. Numerical solution in Figs. 9a–9d gives a thickness of 5.0–5.5%, which is in good agreement with analytical prediction.

Summary and Conclusions

In the present paper, direct numerical simulation was performed to study the effect of an acoustic disturbance source in the presence of a mean shear flow in a two-dimensional duct. Results show good agreement with analytical predictions of Wang and Kassoy.[7] Several interesting features associated with this problem have been observed.

1) There exists a critical frequency above which oblique waves are generated. The interaction between oblique waves and axially traveling waves results in variation of amplitudes of acoustic pressure.

2) Amplified oblique waves that are nearly transverse due to resonant disturbances are observed for the first time. The rate of amplification of these waves is much higher than that of the axially traveling waves. At certain locations of the domain, this strong nearly transverse wave interacts with the axial wave, causing a dramatic change in both wave amplitude and phase.

3) For resonant disturbances with several transversal spatial modes, the growth rate varies significantly for different modes, being the highest for the first transverse mode.

4) The present simulation resolved the acoustic boundary layer very well. The thickness estimated through numerical simulation is in agreement with that predicted by theory.

Acknowledgments

The research presented in this paper was sponsored by the Air Force Office of Scientific Research through Grant AFOSR F-49620-92-J045 and monitored by Mitat Birkan. The authors acknowledge computer support on the Cray C-90 provided by the San Diego Supercomputing Center. The authors are grateful to M. Baum and T. J. Poinsot for permitting them to use their two-dimensional code in the present study. Fruitful discussions with D. R. Kassoy are gratefully acknowledged. The authors express their thanks to an anonymous referee who highlighted the significance of the cross-stream position-dependent acoustic source function.

References

[1]Price, E. W., "Experimental Observations of Combustion Instability," *Fundamentals of Solid-Propellant Combustion*, edited by K. K. Kuo and M. Summerfield, Vol. 90, Progress in Astronautics and Aeronautics, AIAA, New York, 1978, pp. 733–790.

[2]Givi, P., "Model-Free Simulations of Turbulent Reactive Flows," *Progress in Energy and Combustion Science*, Vol. 15, No. 1, 1989.

[3]Pridmore-Brown, D. C., "Sound Propagation in a Fluid Flowing Through an Attenuating Duct," *Journal of Fluid Mechanics*, Vol. 4, 1958, pp. 393–406.

[4]Munger, P., and Gladwell, G. M., "Acoustic Wave Propagation in a Sheared Flow Contained in a Duct," *Journal of Sound and Vibration*, Vol. 9, 1969, pp. 28–48.

[5]Hersh, A. S., and Catton, I., "Effect of Shear Flow on Sound Propagation in Rectangular Ducts," *Journal of the Acoustical Society of America*, Vol. 50, No. 3, 1971, pp. 992–1003.

[6]Baum, J. D., and Levine, J. N., "Numerical Investigation of Acoustic Refraction," *AIAA Journal*, Vol. 25, No. 12, 1987, pp. 1577–1586.

[7]Wang, M., and Kassoy, D. R., "Transient Acoustic Processes in a Low-Mach Number Shear Flow," *Journal of Fluid Mechanics*, Vol. 238, 1992, pp. 509–536.

[8]Culick, F. E. C., and Yang, V., "Prediction of the Stability of Unsteady Motions in Solid Propellant Rocket Motors," *Nonsteady Burning and Combustion Stability of Solid Propellants*, edited by L. DeLuca, E. W. Price, and M. Summerfield, Vol. 143, Progress in Astronautics and Aeronautics, AIAA, Washington, DC, 1992, pp. 719–779.

[9]Zinn, B. T., and Powell, E. A., "Nonlinear Combustion Stability in Liquid-Propellant Rocket Engines," *Thirteenth Symposium (International) on Combustion*, 1971, pp. 491–503.

[10]Padmanabhan, M. S., Powell, E. A., and Zinn, B. T., "Predicting Nonlinear Axial Instabilities in Solid Rockets Using Exact and Approximate Solution Techniques," *Sixteenth Symposium (International) on Combustion*, 1977, pp. 1243–1255.

[11]Margolis, S. B., "Nonlinear Stability of Combustion-Driven Acoustic Oscillations in Resonance Tubes," *Journal of Fluid Mechanics*, Vol. 253, 1993, pp. 67–103.

[12]Baum, M., and Poinsot, T. J., "Using Direct Numerical Simulations to Study $H_2/O_2/N_2$ Flames with Complex Chemistry," *Journal of Fluid Mechanics*, Vol. 281, 1994, pp. 1–32.

[13]Lele, S. K., "Compact Finite Difference Schemes with Spectral-Like Accuracy," *Journal of Computational Physics*, Vol. 103, 1992, pp. 16–42.

[14]Poinsot, T., and Lele, S., "Boundary Conditions for Direct Simulation of Compressible Viscous Flows," *Journal of Computational Physics*, Vol. 101, 1992, pp. 104–129.

[15]Thompson, K., "Time-Dependent Boundary Conditions for Hyperbolic Systems II," *Journal of Computational Physics*, Vol. 89, 1990, pp. 439–461.

[16]Mu, S., M.S. Thesis, Univ. of Colorado, Boulder, CO, 1994.